A Combination of VSG and Amended Fractional-Order Repetitive Control for Improving Power Quality of Grid-Connected Inverter

Hamed Mohammad Kazemi, Ebrahim Afjei
Department of Electrical Engineering
Shahid Beheshti University
Tehran, Iran
h.mohammadkazemi@mail.sbu.ac.ir, e-afjei@sbu.ac.ir

Ali Rahmati
School of Engineering
University of Applied Sciences Upper Austria
Wels, Austria
ali.rahmati.ei@gmail.com

***Abstract*—Nowadays, in the modern power systems, due to increasing the application of renewable energy sources, power inverters are most commonly used electronic devices in the energy systems for ac/dc power conversion. Since the standard power inverters have extremely low inertia elements, the modern power systems meet insufficiency inertia to maintain the grid stability. In virtual synchronous generator (VSG) technique, virtual inertia is emulated in the power inverters by implementing swing equation and as a result, grid inertia is increased and grid stability will be satisfied. Although grid inertia issue is solved by VSG control, dealing with some power quality problems, such as grid current harmonic, which occurs in bad situations, has not been considered in this control theory. In this paper, a control approach based on a combination of VSG technique and amended fractional-order repetitive control (AFORC) is presented for grid-connected inverters to cope with the mentioned problem. The results of simulation studies proved that the proposed method besides fulfilling the main VSG objectives, such as transient frequency response enhancement and increasing total inertia of the power systems, it also can extremely diminish harmonic components of the current injected to the grid in the presence of distorted grid voltage and unbalanced nonlinear rectifier loads.**

Index Terms*—virtual synchronous generator; repetitive control; virtual inertia; harmonic suppression; power quality.

I. Introduction

The growth of renewable energy sources in power systems has increased the grid-connected inverters in order to reduce environmental pollutions, fossil fuels usage and grid losses [1]. Despite the turbines and synchronous machines, which can store kinetic energy and withstand system disturbances because of having inertia in their rotating masses, inverters do not have moving parts, damping property and mechanical components, and as a result, they are called inertia-less devices. Therefore, in modern power systems, which are expanded by renewable energy sources, the grid frequency stability is not guaranteed due to insufficient total inertia [2].

A solution to cope with grid frequency stability problem is that grid-connected inverters mimic synchronous generator (SG) characteristics. In this theory, which is known as virtual synchronous generator (VSG) [3, 4], inverters behave like synchronous generators by emulating the swing equation in control system[5]. In [6, 7], mathematical model of VSG has been explained; these papers have introduced a round rotor machine for VSG model without considering damper windings in the rotor, magnetic-saturation effects in the iron core and eddy currents. Parameter design of VSG without trial and error can be determined by using proposed approach in [8]. Some synchronization methods have been suggested in [9, 10] to improve dynamic response of VSG during grid connection. In [11], operation of VSG under grid fault and improvement in transient response has been described by implementing output current limiting. Dynamic frequency of microgrid during loading transitions and fault events was studied in [12] through a comparative approach to prove that dynamic frequency stability of VSG control performs better than conventional droop control theory.

Many other articles like the above, focused on how to improve the performance of VSG such as transient response for fault contingency, synchronizing methods, parameter designing, achieving closest modeling to the synchronous generator (SG) and so on, but, few researches have been done on maintaining VSG performance to keep injecting sinusoidal current to the grid in presence of abnormal grid voltage condition and different types of local loads. For instance, we can refer to [13] in which by combination of VSG model with the second-order generalized integrator (SOGI), the impact of unbalanced grid voltage on VSG self-synchronization accuracy has been eliminated. In [14], a combination of positive-sequence current adjuster with Decoupled-Double-Synchronous Reference-Frame (DDSRF) PLL for VSG has been proposed to eliminate the produced negative-sequence current and ensure the balanced output current under unbalanced grid voltage. With the proposed strategy in [15], a grid-connected VSG, which is able to supply nonlinear local load power, can reduce harmonic of the current injected to the grid with considering load current in reference current signal of inner current loop control system.

This paper presents a combination method between VSG and amended fractional order repetitive control (AFORC) in which not only can enhance the frequency stability of the

978-1-7281-1334-0/19/$31.00 ©2019 IEEE

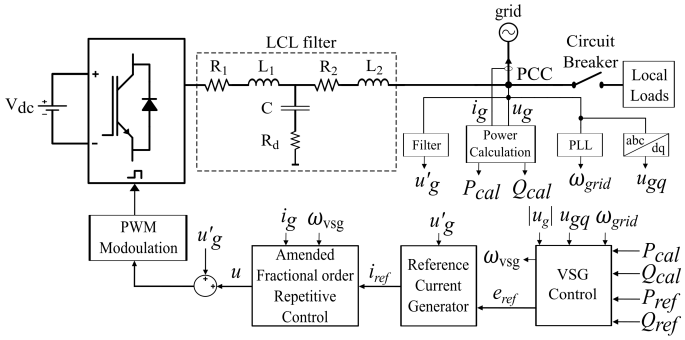

Fig. 1. Single line diagram of electrical and control system.

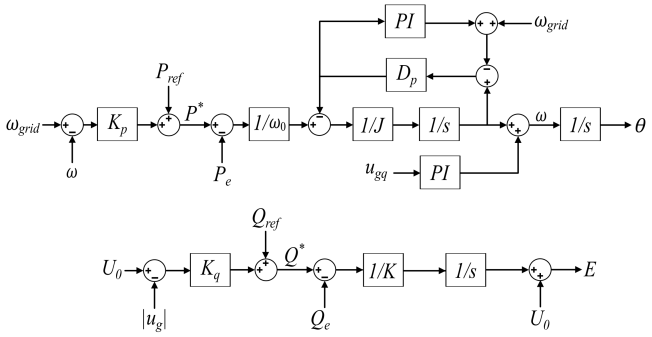

Fig. 2. Block diagram of VSG control system.

system by implementing virtual inertia, but also even in presence of distorted grid voltage and unbalanced nonlinear rectifier loads, AFORC forces grid current to be balance and sinusoidal; therefore, effect of the local load and grid voltage harmonic on the current injected to the grid can be suppressed, and thus, DG provides the grid reference power and required unbalanced nonlinear load current.

II. System Structure and Control Design

A. Electrical Configuration

In Fig. 1, the renewable energy source (V_{dc}) connected to the grid through three-phase inverter and LCL filter, the local load contains single and three phase rectifier loads, and the mentioned signals u_g and i_g are the grid voltage and current, respectively.

B. VSG Control Scheme

The VSG model includes active and reactive power control loops. The virtual inertia is added to inverter, frequency and phase of the e_{ref} is provided, and the actual output active power follows its set point value by implementing swing equation in active power loop. The reactive power loop, which is derived from primary voltage regulation, provides amplitude of the e_{ref} and controls the actual output reactive power [6]. These loops are shown in Fig. 2 and their corresponding equations can be written as (1).

$$\begin{cases} (P^* - P_e)\dfrac{1}{\omega_0} - D(\omega - \omega_g) = J.s.\omega \\ P^* = (\omega_g - \omega)K_p + P_{ref} \\ (Q^* - Q_e)\dfrac{1}{K.s} + U_0 = E \\ Q^* = (U_0 - |u_g|)K_q + Q_{ref} \end{cases} \tag{1}$$

Where P_{ref} and Q_{ref} are the desired output active and reactive powers, respectively, P_e and Q_e are the actual output active and reactive powers, respectively, ω and ω_g are the actual and grid angular frequencies of the rotor, respectively, D is virtual damping factor, J is the moment of inertia of the active power control, U_0 and E are the rated and inner voltage signals, K is the voltage integral coefficient, and K_p and K_q are droop frequency and voltage coefficients.

C. Reference Current Generator

As we have seen above, the output reference signal of VSG is voltage-type, therefore, the Reference Current Generator (RCG) should be used to provide current-type input reference signal for current controller.

$$i_{ref} = (e_{ref} - u_{PCC}).(\frac{1}{L_s.s + R_s}) \tag{2}$$

Where i_{ref} and e_{ref} are the reference current and voltage signals, respectively, L_s is the stator inductance, and R_s is the stator resistance.

D. Amended Fractional-Order Repetitive Control (AFORC)

The AFORC structure is shown in Fig. 3. $i_{err}(z)$ and $D(z)$ are the current tracking error and repetitive disturbances, respectively. To simplify RC design, stabilization of the original plant $P(z)$ with an inner PI current controller $C(z)$, which it also affords sufficient bandwidth for improving RC performance, has to be the first step of RC designing. It should be noted that the unit delay of a digital controller $(1/z)$ has been considered in $P(z)$. Hence, the stabilized plant $G(z)$ is as follows,

$$G(z) = \frac{C(z)P(z)}{1 + C(z)P(z)} \tag{3}$$

In the RC structure $R(z)$, N represents the number of samples in one fundamental period of the input signal, z^{-N} is the time delay unit, z^L is the phase lead term to compensate $S(z)G(z)$ phase lag, K_r is the repetitive gain to regulate the

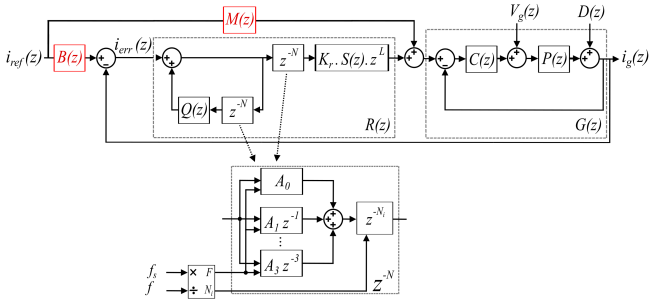

Fig. 3. Block diagram of AFORC control system.

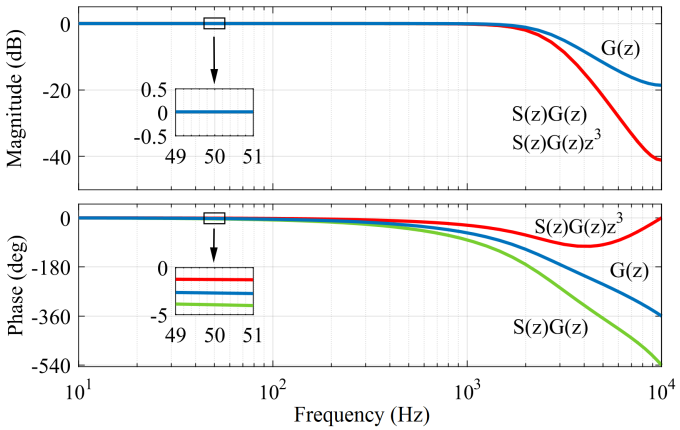

Fig. 4. Bode plot of $G(z)$, $S(z)G(z)$ and $S(z)G(z)z^{+3}$.

stability margin, $Q(z)$ is chosen as either to be close to unity gain or, the same as $S(z)$, to be designed as a second-order low-pass filter to suppress the high-frequency harmonics and improve system stability [16, 17].

$$R(z) = \frac{K_r z^{-N+L} S(z)}{1 - Q(z).z^{-N}} \tag{4}$$

Though the above mentioned RC structure is suitable for most applications, in real systems, grid frequency does not exactly meet 50Hz and fluctuates around it; therefore, the order $N = f_s/f$ is not always integer. Further, VSG control deals with frequency regulation and inertia deficiency problems, hence, it is crucial to have control system that behaves accurately under grid frequency variation. Therefore, achieving this without employing fractional-order for time delay unit will not be possible. In this method, the time delay unit z^{-N} would be approximated by $z^{-(N_i+F)}$ which its integer and fractional delay parts are $z^{-N_i}(N_i = [N])$ and $z^{-F}(F = N - N_i)$, respectively. By the use of Lagrange interpolation, the fractional delay (FD) z^{-F} can be written as [18]:

$$z^{-F} \approx \sum_{k=0}^{n} A_k z^{-k} \tag{5}$$

Where n is the polynomial degree, and Lagrange factor A_k is shown as follows,

$$A_k = \prod_{\substack{i=0 \\ i \neq k}}^{n} \frac{F-i}{k-i} \qquad i,k = 0,1,2,\ldots,\ n \tag{6}$$

According to the Fig. 3, the transfer function from error $i_{err}(z)$ to reference $i_{ref}(z)$ and disturbance signals $d(z)$ signals could be written as,

$$\begin{aligned} i_{err}(z) = {} & \frac{W(z)\left(1 - Q(z)z^{-N}\right) i_{ref}(z)}{1 - z^{-N}H(z)\sum_{k=0}^{n} A_k z^{-k}} \\ & + \frac{\left(1 - Q(z)z^{-N}\right) d(z)}{1 - z^{-N}H(z)\sum_{k=0}^{n} A_k z^{-k}} \end{aligned} \tag{7}$$

Where $W(z) = B(z) - M(z)G(z)$, $H(z) = Q(z) - K_r z^{+L} S(z)G(z)$ and characteristic equation can be expressed as,

$$1 - z^{-N}H(z)\sum_{k=0}^{n} A_k z^{-k} = 0 \tag{8}$$

If the following two conditions hold, the system stability is satisfied:

1) The roots of $1 + C(z)P(z) = 0$ should be inside of unit circle of z domain.
2) The roots of $1 - z^{-N}H(z)\sum_{k=0}^{n} A_k z^{-k} = 0$ should be inside of unit circle of z domain.

As we can see the bode diagram of $G(z)$ in Fig. 4, the PI controller $C(z)$ with coefficient values $K_p = 0.06$ and $K_i = 0.45$ stabilizes the original plant transfer function $P(z)$. Thus, all the poles of $G(z)$ are within a unit circle of z domain and as a result first RC stability condition is satisfied.

The second stability condition will be satisfied if the (9) holds in all frequencies.

$$\left| H(z)\sum_{k=0}^{n} A_k z^{-k} \right| < 1 \tag{9}$$

From the above, in order not to restrict maximum acceptable value of the $|H(z)|$ and have no difficulty in RC parameter selection, the FD magnitude should be close to unity and not much more in whole frequency range. Also, for achieving good system performance, FD must have sufficient bandwidth. As the bode diagram of FD for orders $n = 1$ to $n = 4$ with different fractional values $(F = 0,\ 0.1, \ldots,\ 0.9)$ have been shown in Fig. 5, straightforwardly by considering the above conditions, the order $n = 3$ with the bandwidth of 75% Nyquist frequency and close magnitude to unity is the best choice for polynomial degree. It should be noted that increasing the order from 4 to

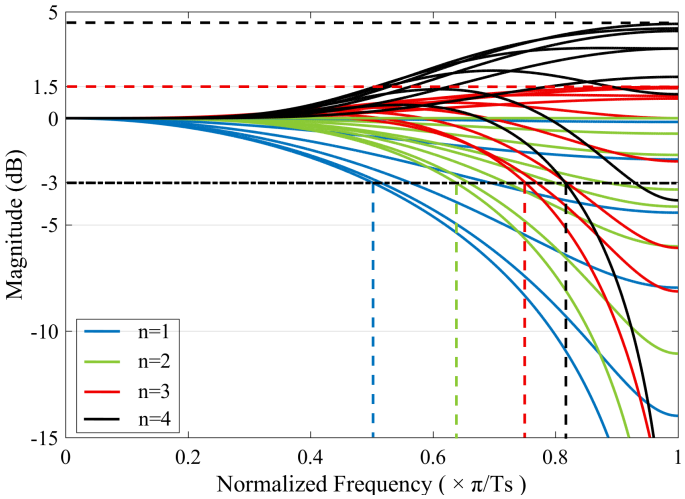

Fig. 5. Frequency response of Lagrange interpolation based FD filters.

more, results a high FD magnitude at high frequencies which are not acceptable regarding the above description.

From Fig. 5, it can be realized that the maximum value of FD for $n = 3$ is about 1.19 (1.5 dB). Hence, the worst case satisfying second stability condition is written as below,

$$|H(z)| < 0.84 \tag{10}$$

In the next step, the second-order low-pass filter $Q(z)$ is designated to enhance the robustness of RC, and to suppress the high-frequency harmonics and magnitude compensation for $G(z)$, we should adopt another second-order low-pass filter $S(z)$. They can be chosen as,

$$Q(z) = \frac{0.15z^2 + 0.35z + 0.04}{z^2 - 0.55z + 0.10} \tag{11}$$

$$S(z) = \frac{0.11z^2 + 0.29z + 0.04}{z^2 - 0.74z + 0.20} \tag{12}$$

To compensate the phase lag of $S(z)G(z)$ and RC loop, the time advance unit z^{+L} should be added to the RC. The bode diagram of $S(z)G(z)$ which is shown in the Fig. 4, demonstrates that z^{+3} is appropriate phase lead compensator.

K_r is the last remaining parameter of $H(z)$ to be selected. According to (10), the acceptable range of AFORC gain is $0 < K_r \leq 1.81$. As it is clear in the Fig. 6, the vector $H(z)$ does not exceed 0.84, and then, both stability conditions are fulfilled and control system becomes stable.

In conventional RC structures, $B(z)$ and $M(z)$ are not considered, and achieving to lowest magnitude of $H(z)$ is the only way to attenuate the current error signal $i_{err}(z)/i_{ref}(z)$. But according to (7), in the proposed AFORC structure to more diminish $i_{err}(z)/i_{ref}(z)$, one can try to decrease the vector $W(z)$ as well as $H(z)$. Obviously, in conventional RC, the numerator of $i_{err}(z)/i_{ref}(z)$ includes $(1-G(z))$ instead of

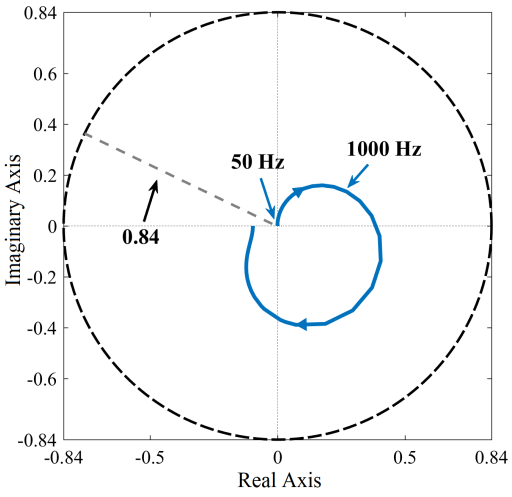

Fig. 6. Nyquist plot of $H(z)$.

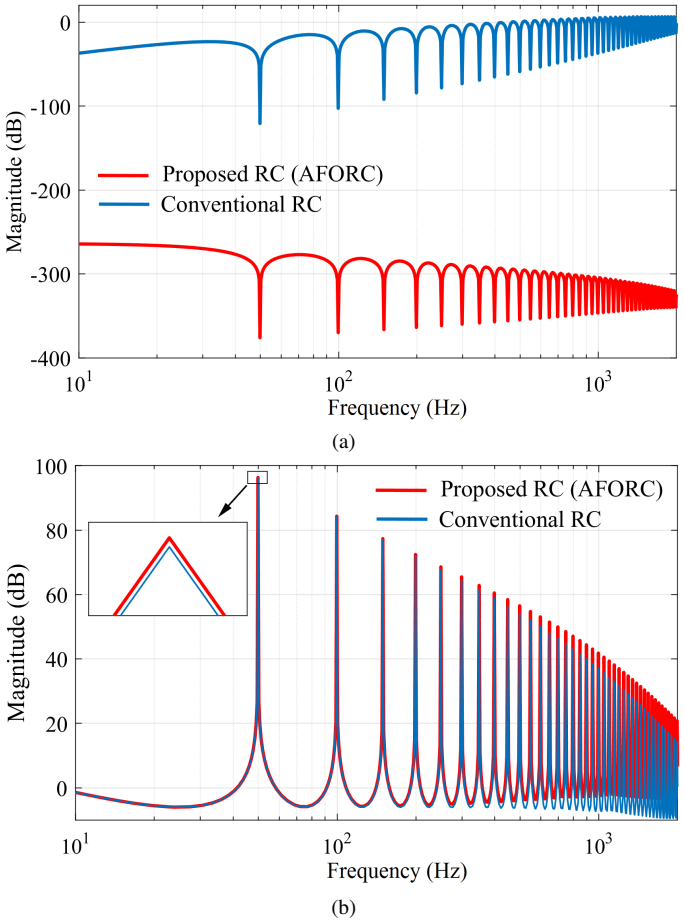

Fig. 7. Comparison of conventional RC and AFORC a) Error characteristic b) Open loop gain

$(B(z) - M(z)G(z))$.

In this paper, we suggest that $B(z)$ and $M(z)$ have to be chosen in such a way that $W(z)$ becomes zero. In order to achieve this purpose, $B(z)$ should be considered as $M(z)G(z)$. On the other hand, $B(z)$ can affect phase and magnitude of $i_{ref}(z)$, which is not desired. Clearly, the $i_{ref}(z)$ only has fundamental frequency term, and according to phase response in Fig. 4, $G(z)$ will have negative impact on reference signal phase. Then, $M(z)$ should be designed as phase lead compensator to eliminate the effect of $G(z)$ in a fashion to $B(z)$ has no phase shift at fundamental frequency similar to magnitude response of $G(z)$, which does not affect amplitude of $i_{ref}(z)$. Thus, $B(z)$ does not have any effect on phase and amplitude of $i_{ref}(z)$ at fundamental frequency, and $M(z)$ can be written as follows,

$$M(z) = \frac{2.107(z - 0.862)}{z - 0.7092} \tag{13}$$

Fig. 7 proves that recent modification in RC structure suppresses the magnitude of error signal about 3 times (in dB) more than the conventional RC without decreasing open loop gain and command following capability.

III. Simulation Results

To verify validity of the proposed control approach, simulation studies are carried out in MATLAB/Simulink environment. The rated grid voltage is 380V, rated frequency is 50Hz, rated power of three-phase inverter is 25kVA, sampling and inverter switching frequencies are set as 20kHz, the local load consists of three phase nonlinear rectifier load with $R_1 = 15\Omega$ and $C_1 = 2000\mu$F, and single phase nonlinear rectifier load with $R_2 = 35\Omega$ and $L_2 = 27$mH.

A. System Performance with Combination of VSG and PI Controllers

Fig. 8 shows the system performance with combination of VSG and PI controllers under unbalanced nonlinear local loads and distorted grid (voltage THD is 4.5%). As seen in Fig. 8, VSG and PI are not appropriate controllers for harmonic suppression and the grid current have harmonic terms inevitably. In this case, inverter injects 15KW active power to the grid and injected current THD is 5.43% .

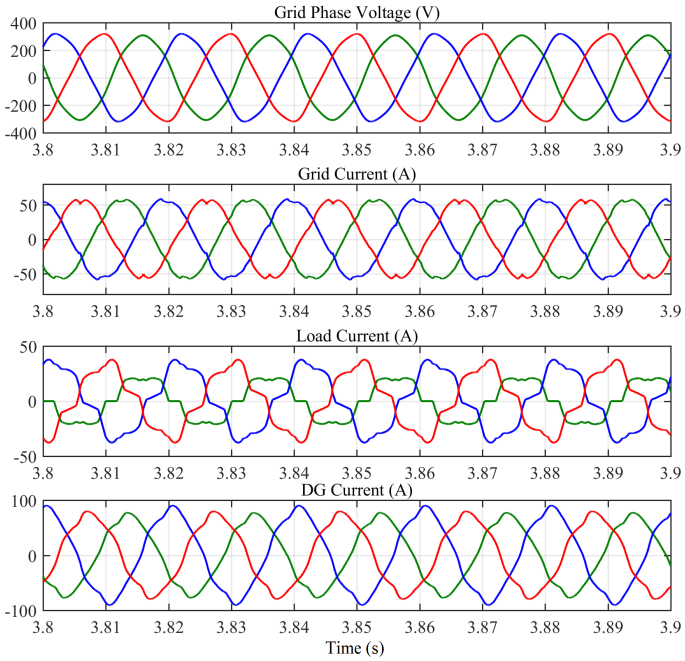

Fig. 8. System Performance with Combination of VSG and PI Controllers

B. System Performance with Combination of VSG and AFORC

At first, inverter injects 15KW active power to the distorted grid (voltage THD is 4.5%) by employing VSG and AFORC. At $t = 2s$, the grid frequency drops from 50Hz to 49.7Hz, but because of the emulated inertia, inverter frequency decreases smoothly and the inverter responds to the frequency change by

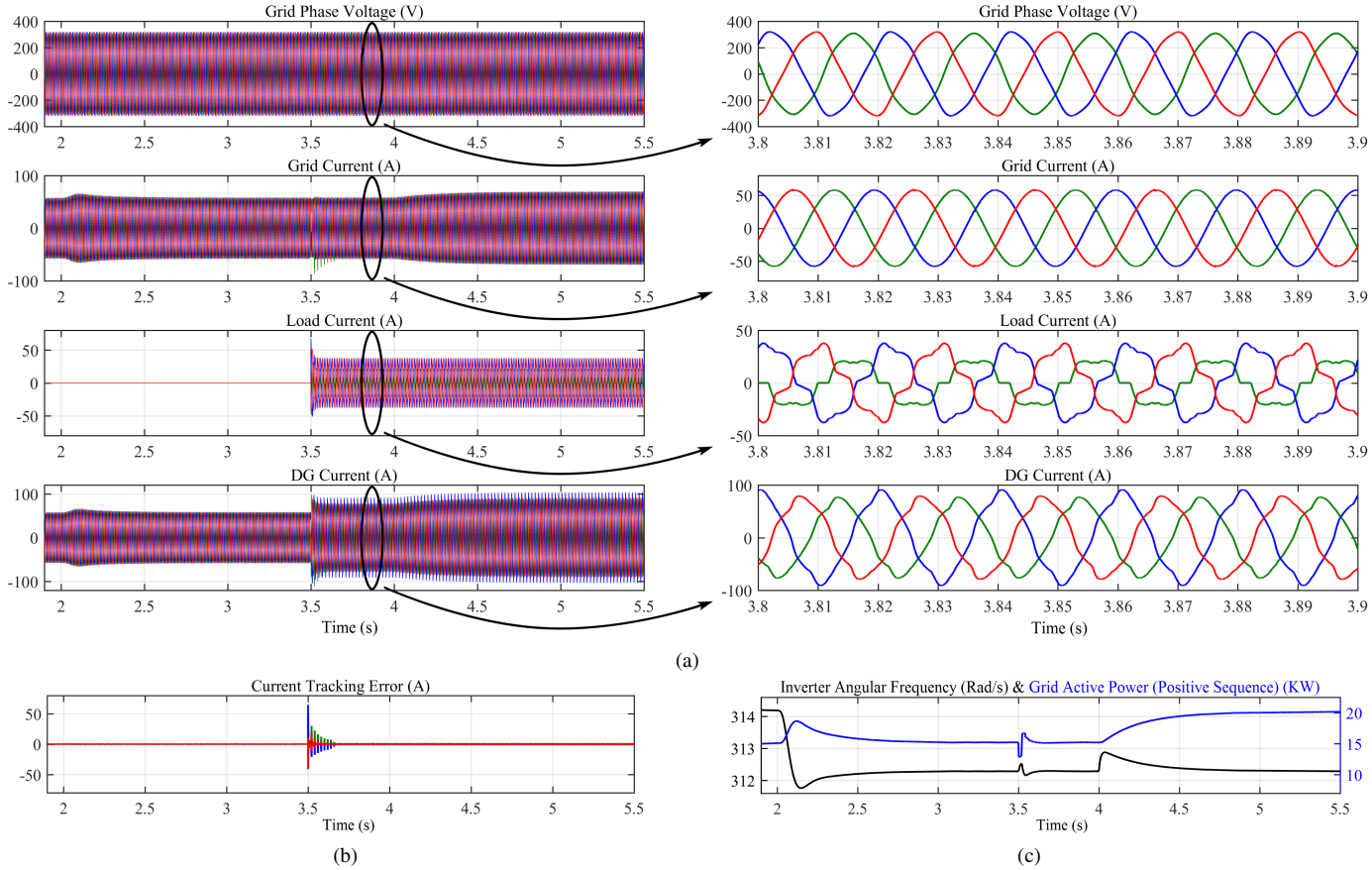

(a)

(b)

(c)

Fig. 9. System Performance with Combination of VSG and AFORC a) Grid voltage and current, and load and DG currents b) Current tracking error c) Inverter angular frequency and grid active power

injecting active power to the grid in the early moments (Fig. 9c). When the unbalanced nonlinear loads are connected to the system at $t = 3.5s$, current tracking error signal has great value in the early periods, but it diminishes step by step and after 9 time periods, i_{err} is highly suppressed (Fig. 9b). In this case, grid current THD is 0.67%. As seen in Fig. 9 (b), since the grid active power is still 15KW after local loads connection, the local loads are supplied by inverter. At $t = 4s$, reference active power is set to 20KW, but the same as frequency reduction, inverter responses gradually to the change and grid active power reaches to its set point after $1.5s$ accordingly.

IV. Conclusion

In this paper, in order to VSG can deal with power quality problem, such as grid current harmonic, along with transient frequency response improvement, an amended fractional order repetitive controller has been applied to VSG control approach. The simulation results illustrate that recommended control system can not only behave similar to synchronous generator, but also it can supply unbalanced nonlinear rectifier loads and keep injecting sinusoidal and balanced current to the grid even facing grid voltage distortion.

References

[1] G. Pepermans, J. Driesen, D. Haeseldonckx, R. Belmans, and W. D'haeseleer, "Distributed generation: definition, benefits and issues," Energy Policy, vol. 33, no. 6, pp. 787-798, 2005/04/01/ 2005.

[2] B. Kroposki et al., "Achieving a 100% Renewable Grid: Operating Electric Power Systems with Extremely High Levels of Variable Renewable Energy," IEEE Power and Energy Magazine, vol. 15, no. 2, pp. 61-73, 2017.

[3] J. Driesen and K. Visscher, "Virtual synchronous generators," in 2008 IEEE Power and Energy Society General Meeting - Conversion and Delivery of Electrical Energy in the 21st Century, 2008, pp. 1-3.

[4] H. Bevrani, T. Ise, and Y. Miura, "Virtual synchronous generators: A survey and new perspectives," International Journal of Electrical Power & Energy Systems, vol. 54, pp. 244-254, 2014/01/01/ 2014.

[5] M. P. N. v. Wesenbeeck, S. W. H. d. Haan, P. Varela, and K. Visscher, "Grid tied converter with virtual kinetic storage," in 2009 IEEE Bucharest PowerTech, 2009, pp. 1-7.

[6] Q. C. Zhong and G. Weiss, "Synchronverters: Inverters That Mimic Synchronous Generators," IEEE Transactions on Industrial Electronics, vol. 58, no. 4, pp. 1259-1267, 2011.

[7] Q. C. Zhong and G. Weiss, "Static synchronous generators for distributed generation and renewable energy," in 2009 IEEE/PES Power Systems Conference and Exposition, 2009, pp. 1-6.

[8] H. Wu et al., "Small-Signal Modeling and Parameters Design for Virtual Synchronous Generators," IEEE Transactions on Industrial Electronics, vol. 63, no. 7, pp. 4292-4303, 2016.

[9] Q. C. Zhong, P. L. Nguyen, Z. Ma, and W. Sheng, "Self-Synchronized Synchronverters: Inverters Without a Dedicated Synchronization Unit," IEEE Transactions on Power Electronics, vol. 29, no. 2, pp. 617-630, 2014.

[10] J. Wu, F. Zhuo, Z. Wang, H. Yi, and K. Yu, "Pre-synchronization method for grid-connection of virtual synchronous generators based micro-grids," in 2017 19th European Conference on Power Electronics and Applications (EPE'17 ECCE Europe), 2017, pp. P.1-P.8.

[11] K. Shi, H. Ye, P. Xu, D. Zhao, and L. Jiao, "Low-voltage ride through control strategy of virtual synchronous generator based on the analysis of excitation state," IET Generation, Transmission & Distribution, vol. 12, no. 9, pp. 2165-2172, 2018.

[12] J. Liu, Y. Miura, and T. Ise, "Power Quality improvement of microgrids by virtual synchronous generator control," in 2016 Electric Power Quality and Supply Reliability (PQ), 2016, pp. 119-124.

[13] X. Wang and D. Sun, "Multi-objective self-synchronised virtual synchronous generator in unbalanced power grid," Electronics Letters, vol. 54, no. 12, pp. 779-781, 2018.

[14] X. Zheng, C. Wang and S. Pang, "Injecting positive-sequence current virtual synchronous generator control under unbalanced grid," in IET Renewable Power Generation, vol. 13, no. 1, pp. 165-170, 7 1 2019.

[15] Z. Qu, H. Yang, Y. Cai and H. Wang, "Application of virtual synchronous generator technology in three-phase four-leg inverter," 2017 20th International Conference on Electrical Machines and Systems (ICEMS), Sydney, NSW, 2017, pp. 1-6.

[16] M. Zhang, L. Huang, W. Yao, and Z. Lu, "Circulating Harmonic Current Elimination of a CPS-PWM-Based Modular Multilevel Converter With a Plug-In Repetitive Controller," IEEE Transactions on Power Electronics, vol. 29, no. 4, pp. 2083-2097, 2014.

[17] Z. Kai, K. Yong, X. Jian, and C. Jian, "Direct repetitive control of SPWM inverter for UPS purpose," IEEE Transactions on Power Electronics, vol. 18, no. 3, pp. 784-792, 2003.

[18] R. Nazir, K. Zhou, N. Watson, and A. Wood, "Analysis and synthesis of fractional order repetitive control for power converters," Electric Power Systems Research, vol. 124, pp. 110-119, 2015/07/01/ 2015.